*Progress In Electromagnetics Research C, Vol. 108, 159–169, 2021*

# A Tri-Band Negative Group Delay Circuit for Multiband Wireless Applications

**Yuwei Meng, Zhongbao Wang*, Shaojun Fang, and Hongmei Liu**

**Abstract**—A tri-band negative group delay (NGD) microwave circuit for multiband wireless applications is proposed and self-matched without the need for external matching networks. The frequency range can be influenced by the characteristic impedance of the microstrip lines. Under the condition that the microstrip circuit can be implemented with the common printed circuit board (PCB) fabrication technology, the frequency ratio of the highest NGD band to the lowest NGD band can vary between 3.8 and 10.9. For verification, a 1.2/3.5/5.8-GHz tri-band NGD circuit for Beidou B2, WiMax, and WLAN applications is designed, fabricated, and measured. From the measured results, the NGD times are −1.08 ns, −1.19 ns, and −1.09 ns at three NGD central frequencies with insertion losses of 16.4 dB, 24.6 dB, and 18.9 dB, respectively. And the measured NGD bandwidths are 12.40% for the lower band, 8.60% for the center band, and 3.59% for the upper band, in which the return losses are greater than 16 dB.

## 1. INTRODUCTION

Group delay (GD) distortion in a circuit or system inevitably distorts the signal by introducing inter-symbol interference, thereby degrading the overall system performance. Recently, negative group delay circuit (NGDC) has been used to compensate the GD variations, which can avoid signal distortion and recover the signal integrity [1, 2]. Furthermore, NGDC has attracted much attention because of its abnormal electromagnetic wave propagation characters and wide application prospects. Nowadays, the NGDCs have been applied to group delay equalization of ultra-wideband amplifiers [3, 4], linear-phase filters [5, 6], efficiency enhancement of feed-forward amplifiers [7], and elimination of phase variation with frequency in phase shifter [8].

NGD microwave circuit was first proposed in [9], after which many improved structures appeared, such as miniaturization [10, 11] and insertion loss (IL) reduction [12, 13]. In addition, many other methods to achieve NGD characteristics are proposed [14–17]. In [14], the filter theory is applied to design an NGDC with the characteristics of flat. And transversal-filter topologies based on amplifiers are discussed in [15]. Recently, the signal interference technique starts to be studied since its flexibility and simplicity in design [16, 17].

With the rapid development of various wireless systems for multiple-access and multi-functional applications, multiband components have drawn more attention, such as multiband power dividers [18], antennas [19], and filters [20]. Compared to the conventional combination of mono-band blocks, multiband components have the advantages of lower size and easier realization in practice particularly when many bands are involved. To satisfy the GD compensation for multiband devices, the design approaches of multiband NGDCs are attractive. The first dual-band NGDC was proposed in [21], which was designed with composite right/left-handed $\lambda/4$ short stubs. In order to achieve miniaturization, some structures were presented in [22–25]. However, the circuits in [22, 23] had poor return loss

*Received 22 November 2020, Accepted 29 December 2020, Scheduled 11 January 2021*
* Corresponding author: Zhongbao Wang (wangzb@dlmu.edu.cn).
The authors are with the School of Information Science and Technology, Dalian Maritime University, Dalian, Liaoning 116026, China.

performances. A dual-band NGDC with low signal-attenuation and arbitrary frequency ratio was proposed in [26]. However, only two NGD working bands were obtained in these NGDCs [21–26]. To increase the number of NGD working bands, three multiband NGDCs were designed in [27–29]. The circuit in [27] consisted of three independent resonators cascaded, and three NGD bands of the NGDC can be controlled separately. In [28, 29], the multiband NGD was obtained by taking advantage of the periodic effects of the circuit itself. However, the existing multiband NGDCs cannot directly obtain good input- and output-port impedance matching characteristics. Therefore, external matching networks are needed. Certainly, the use of external matching networks will increase the number of components and the size of circuits.

In this paper, a novel tri-band NGDC without the need for external matching networks is proposed for multiband wireless applications, which has good input- and output-port impedance matching characteristics of the three NGD bands. The proposed circuit consists of three-stage series transmission lines ($Z_1$, $Z_2$, $Z_3$) connecting with two resistors $r_1$, and a resistor $r_2$ connected by two transition lines ($Z_4$). The transmission lines ($Z_1$, $Z_2$, $Z_3$) and resistor $r_1$ constitute a lossy resonator, which has three resonant frequencies. The transmission line $Z_4$ and resistor $r_2$ are used to achieve port matching. The closed design formulas are derived. Both the theoretical and experimental results are given and discussed.

## 2. CIRCUIT STRUCTURE AND THEORY ANALYSIS

The topology of the proposed NGDC is shown in Fig. 1. It is composed of a structure with three-stage series transmission lines with characteristic impedances $Z_1$, $Z_2$, $Z_3$ and electrical lengths $\theta_1$, $\theta_2$, $\theta_3$ connecting with resistors $r_1$, and a resistor $r_2$ inserted between two transmission lines with characteristic impedance $Z_4$ and electrical length $\theta_4$.

For the convenience of analysis, the even- and odd-mode equivalent circuits are shown in Fig. 2. Based on transmission line theory and network analysis, the even- and odd-mode input admittances $Y_{\text{in_odd}}$ and $Y_{\text{in_even}}$ are expressed as

$$Y_{\text{in_odd}} = a_1 + \text{j}a_2, \tag{1a}$$

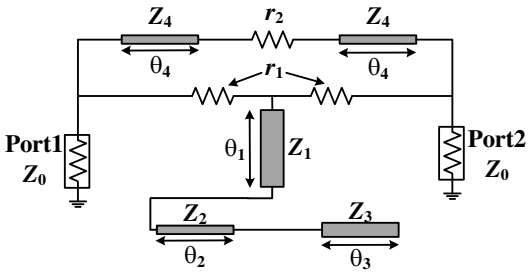


**Figure 1.** Configuration of the proposed NGD microwave circuit.

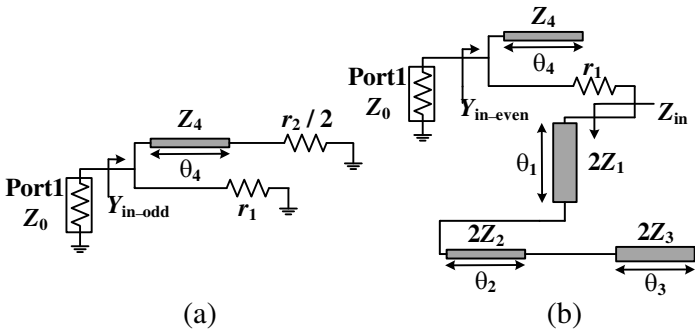


**Figure 2.** Odd- and even-mode equivalent circuits. (a) Odd-mode. (b) Even-mode.

$$Y_{\text{in_even}} = a_3 + \mathrm{j}a_4, \tag{1b}$$

where $a_1$, $a_2$, $a_3$, $a_4$ are given in Equation (2).

$$a_1 = \frac{1}{r_1} + \frac{r_2\left(1+\tan^2\theta_4\right)/2}{\left(r_2/2\right)^2 + Z_4^2\tan^2\theta_4}, \tag{2a}$$

$$a_2 = \frac{\left[\left(r_2/2\right)^2 - Z_4^2\right]\tan\theta_4 \Big/ Z_4}{\left(r_2/2\right)^2 + Z_4^2\tan^2\theta_4}, \tag{2b}$$

$$a_3 = \frac{r_1}{r_1^2 + 4Z_{\text{in}}^2}, \tag{2c}$$

$$a_4 = \frac{\tan\theta_4}{Z_4} - \frac{2Z_{\text{in}}}{r_1^2 + 4Z_{\text{in}}^2}, \tag{2d}$$

$$Z_{\text{in}} = Z_1\frac{Z_1\tan\theta_1\left(Z_2 + Z_3\cot\theta_3\tan\theta_2\right) - Z_2\left(Z_3\cot\theta_3 - Z_2\tan\theta_2\right)}{Z_1\left(Z_2 + Z_3\cot\theta_3\tan\theta_2\right) + Z_2\left(Z_3\cot\theta_3 - Z_2\tan\theta_2\right)\tan\theta_1}, \tag{2e}$$

where $\theta_1 = \theta_2 = \theta_3 = \pi f/(2f_0)$, $\theta_4 = \pi f/f_0$, and $f_0 = (f_1 + f_2)/2$. $f_1$ and $f_2$ are the central frequencies of the lower and upper NGD bands, respectively. $f_0$ is the central frequency of the middle NGD band. Then, the $S$-parameters can be expressed as

$$S_{11} = \frac{Y_0^2 - Y_{\text{in_odd}}Y_{\text{in_even}}}{\left(Y_0 + Y_{\text{in_odd}}\right)\left(Y_0 + Y_{\text{in_even}}\right)}, \tag{3a}$$

$$S_{21} = \frac{Y_0^2\left(Y_{\text{in_odd}} - Y_{\text{in_even}}\right)}{\left(Y_0 + Y_{\text{in_odd}}\right)\left(Y_0 + Y_{\text{in_even}}\right)}, \tag{3b}$$

where $Y_0 = 1/Z_0$, $Z_0$ is the port impedance. According to Equations (1a), (1b), and (3b), $S_{21}$ can be derived as

$$S_{21} = \frac{X_1 + \mathrm{j}X_2}{X_3 + \mathrm{j}X_4}. \tag{4}$$

Then the GD of the proposed circuit can be obtained as

$$\tau = -\frac{\mathrm{d}\angle S_{21}}{\mathrm{d}\omega} = \frac{X_1'X_2 - X_1X_2'}{X_1^2 + X_2^2} - \frac{X_3'X_4 - X_4X_3'}{X_3^2 + X_4^2}, \tag{5}$$

where values of $X_1$, $X_2$, $X_3$, $X_4$, $X_1'$, $X_2'$, $X_3'$, and $X_4'$ are given in Equation (6).

$$X_1 = Y_0\left(a_1 - a_3\right), \tag{6a}$$

$$X_2 = Y_0\left(a_2 - a_4\right), \tag{6b}$$

$$X_3 = \left(Y_0 + a_1\right)\left(Y_0 + a_3\right) - a_2a_4, \tag{6c}$$

$$X_4 = a_2\left(Y_0 + a_3\right) + a_4\left(Y_0 + a_1\right), \tag{6d}$$

$$X_1' = Y_0\left(a_1' - a_3'\right), \tag{6e}$$

$$X_2' = Y_0\left(a_2' - a_4'\right), \tag{6f}$$

$$X_3' = Y_0\left(a_1' + a_3'\right) + a_1'a_3 + a_1a_3' - a_2'a_4 - a_2a_4', \tag{6g}$$

$$X_4' = Y_0\left(a_2' + a_4'\right) + a_2'a_3 + a_2a_3' + a_1'a_4 + a_1a_4', \tag{6h}$$

where $a_1'$, $a_2'$, $a_3'$, $a_4'$, and $Z_{in}'$ are given in Equation (7),

$$a_1' = \frac{r_2\tan\theta_4\left(1+\tan^2\theta_4\right)\left[\left(r_2/2\right)^2 + Z_4^2\tan^2\theta_4 - Z_4^2\left(1+\tan^2\theta_4\right)\right]\tau_4}{\left[\left(r_2/2\right)^2 + Z_4^2\tan^2\theta_4\right]^2}, \tag{7a}$$

$$a_2' = \frac{\left[\left(r_2/2\right)^2 - Z_4^2\right]\left(1+\tan^2\theta_4\right)\left[\left(r_2/2\right)^2 - Z_4^2\tan^2\theta_4\right]}{\left[\left(r_2/2\right)^2 + Z_4^2\tan^2\theta_4\right]^2}, \tag{7b}$$

$$a_3' = \frac{-8r_1 Z_{\text{in}} Z_{\text{in}}'}{\left(r_1^2 + 4Z_{\text{in}}^2\right)^2}, \tag{7c}$$

$$a_4' = \frac{\left(1+\tan^2\theta_4\right)\tau_4}{Z_4} - \frac{2Z_{\text{in}}'\left(r_1^2 - 4Z_{\text{in}}^2\right)}{\left(r_1^2 + 4Z_{\text{in}}^2\right)^2}, \tag{7d}$$

$$Z_{\text{in}}' = \frac{Z_1\left(P-Q\right)}{\left[Z_1\left(Z_2 + Z_3\cot\theta_3\tan\theta_2\right) + Z_2\left(Z_3\cot\theta_3 - Z_2\tan\theta_2\right)\tan\theta_1\right]^2}, \tag{7e}$$

with

$$P = \begin{bmatrix} -Z_2\left(-Z_3\left(1+\cot^2\theta_3\right)\tau_3 - Z_2\left(1+\tan^2\theta_2\right)\tau_2\right) + Z_1Z_2\left(1+\tan^2\theta_1\right)\tau_1 \\ +Z_1Z_3\left(1+\tan^2\theta_1\right)\tau_1\cot\theta_3\tan\theta_2 + Z_1Z_3\tan\theta_1\left(1+\tan^2\theta_2\right)\tau_2\cot\theta_3 \\ -Z_1Z_3\tan\theta_1\tan\theta_2\left(1+\cot^2\theta_3\right)\tau_3 \end{bmatrix}$$
$$\times\left[Z_1\left(Z_2 + Z_3\cot\theta_3\tan\theta_2\right) + Z_2\left(Z_3\cot\theta_3 - Z_2\tan\theta_2\right)\tan\theta_1\right], \tag{8a}$$

$$Q = \begin{bmatrix} Z_1Z_3\left(1+\tan^2\theta_2\right)\cot\theta_3\tau_2 - Z_1Z_3\left(1+\cot^2\theta_3\right)\tau_3\tan\theta_2 \\ +Z_2\left(1+\tan^2\theta_1\right)\tau_1\left(Z_3\cot\theta_3 - Z_2\tan\theta_2\right) \\ +Z_2\tan\theta_1\left(-Z_3\left(1+\cot^2\theta_3\right)\tau_3 - Z_2\left(1+\tan^2\theta_2\right)\tau_2\right) \end{bmatrix}$$
$$\times\left[-Z_2\left(Z_3\cot\theta_3 - Z_2\tan\theta_2\right) + Z_1\tan\theta_1\left(Z_2 + Z_3\cot\theta_3\tan\theta_2\right)\right]. \tag{8b}$$

Based on Equations (3) and (5) at frequencies $f_0$ and $f_1(f_2)$, the six unknown design parameters ($Z_1$, $Z_2$, $Z_3$, $Z_4$, $r_1$, $r_2$) can be solved.

## 3. PARAMETERS ANALYSIS

According to Figs. 3–6, the characteristic impedance of transmission lines can be used to adjust the performance of the proposed NGDC. As can be seen in Fig. 3, the absolute values of NGD time at three NGD central frequencies are proportional to $Z_1$. When $Z_1$ increases, the central frequency of the lower NGD band $f_1$ decreases, and that of the upper NGD band $f_2$ increases. So the frequency ratio of the highest NGD band to the lowest NGD band ($n = f_2/f_1$) is increased. In addition, the IL and port matching are constant at $f_0$. Thus, $Z_1$ could be employed to adjust the NGD time consistency at three frequencies.

Figure 4 gives the analysis of $Z_2$. As observed from these results, $Z_2$ has little effect on the NGD time at $f_0$, while it is proportional to the frequency ratio $f_2/f_1$ and the absolute value of NGD time at $f_1$ and $f_2$. For $|S_{21}|$ and $|S_{11}|(|S_{22}|)$ at three NGD central frequencies, the values remain basically unchanged. From Fig. 5, the impact of $Z_3$ on performance to be opposite to $Z_2$ can be obtained.

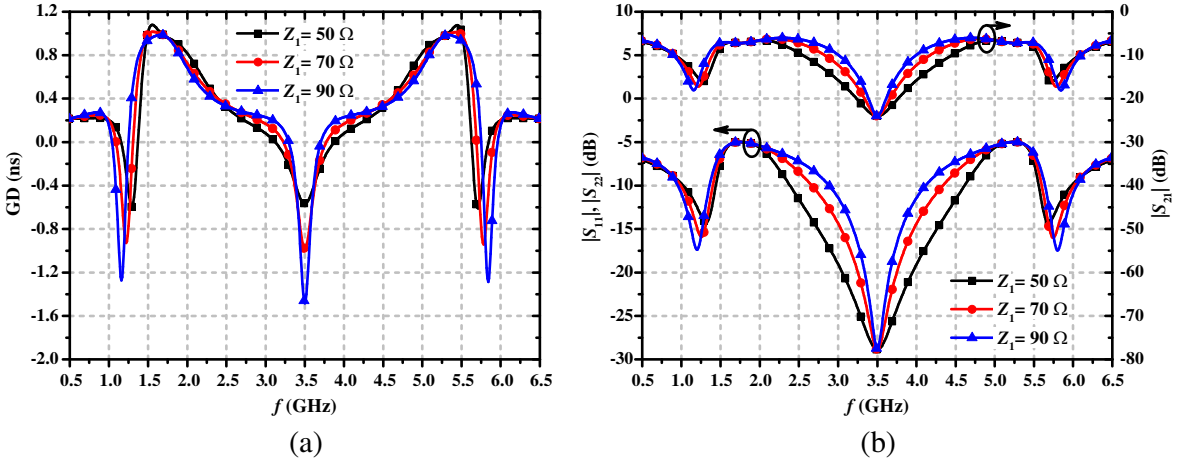


**Figure 3.** Effect of $Z_1$ on the performances of the proposed tri-band NGDC. (a) GD. (b) $S$-parameters.

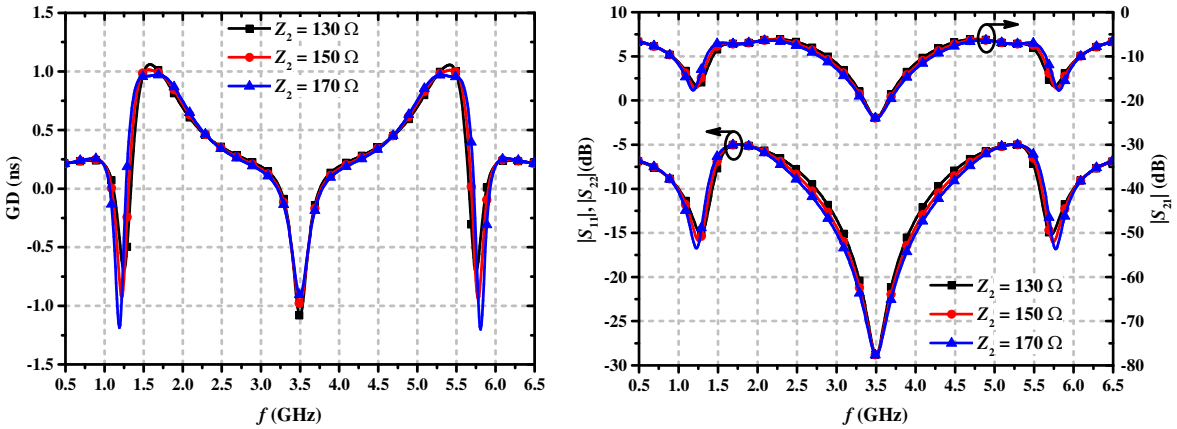


**Figure 4.** Effect of $Z_2$ on the performances of the proposed tri-band NGDC. (a) GD. (b) $S$-parameters.

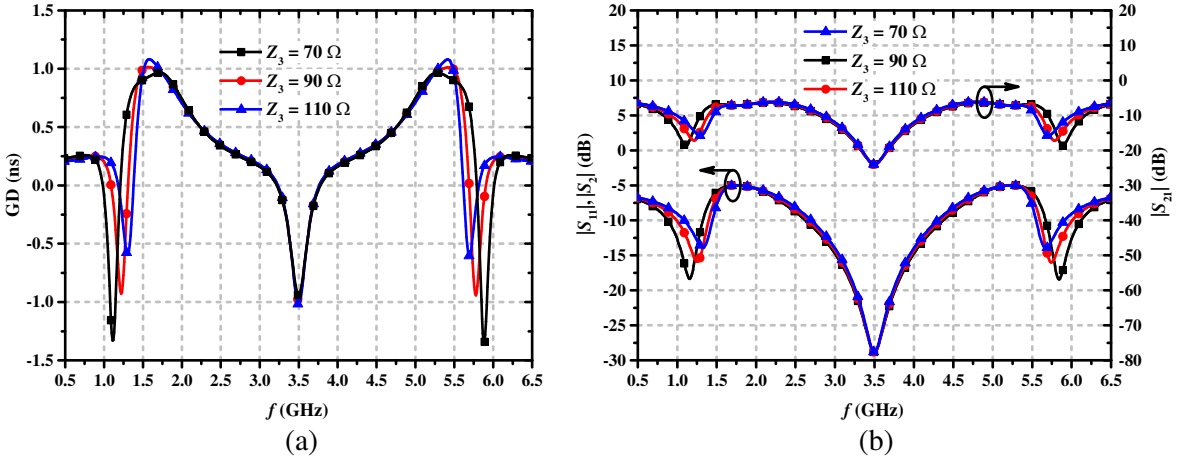


**Figure 5.** Effect of $Z_3$ on the performances of the proposed tri-band NGDC. (a) GD. (b) $S$-parameters.s

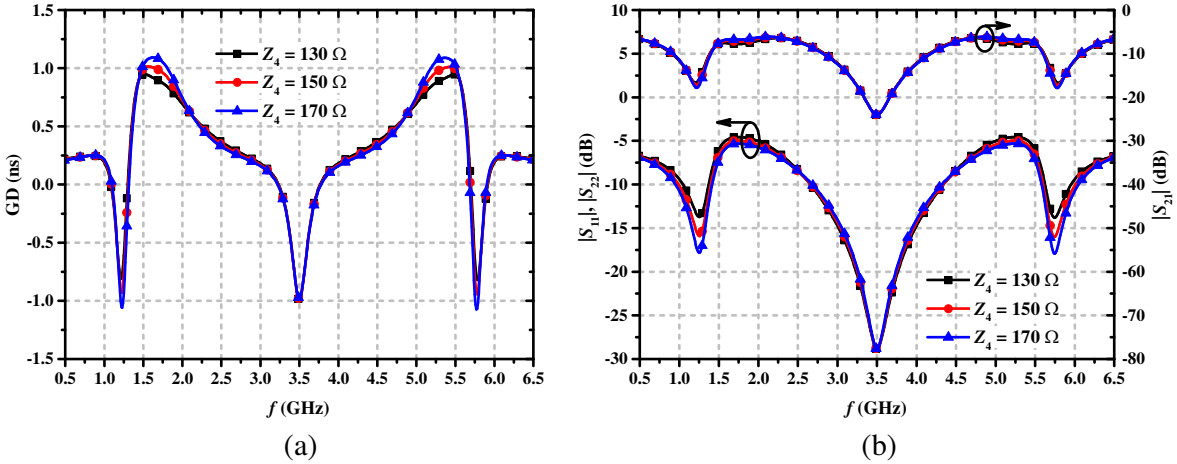


**Figure 6.** Effect of $Z_4$ on the performances of the proposed tri-band NGDC. (a) GD. (b) $S$-parameters.

However, the impact is much greater than $Z_2$. Consequently, through adjusting the values of $Z_2$ and $Z_3$, the desired $f_1$ and $f_2$ can be obtained without influencing the NGD time.

For $Z_4$ in Fig. 6, it is proportional to the absolute value of NGD time at $f_1$ and $f_2$ without any other influence on NGD time at $f_0$. Meanwhile, $|S_{11}|(|S_{22}|)$ decrease as $Z_4$ increases while the IL is unaffected. $Z_4$ is very beneficial for adjusting the absolute value of NGD time at $f_1$ and $f_2$.

According to Figs. 3–5, the frequency ratio can be adjusted by changing the characteristic impedance of the transmission lines. In theory, the proposed NGDC can operate in an arbitrary frequency ratio of the highest NGD band to the lowest NGD band ($f_2/f_1$), but in practice, the construction of the NGDC is also constrained by the range of impedance that can be realized. Based on the trends in Figs. 3–6 and the range of impedance that could be realized, the realizable frequency ratio $f_2/f_1$ can be found from Fig. 7. The electrical parameters are given in Table 1. As can be observed in Fig. 7, the maximum of the frequency ratio is 10.9 (i.e., 6.414/0.588), and the minimum is 3.8 (i.e., 5.532/1.469). For the minimum frequency ratio 3.8, the used value of $Z_1$ in Table 1 is not its minimum value for ensuring the port matching. $S$-parameters at the corresponding frequency are given in Fig. 8. The return losses (RL) are all lower than 10 dB in the NGD bands.

**Table 1.** Electrical parameters of the proposed NGDC with the minimum and maximum frequency ratios.

| Frequency ratio | $Z_1$ ($\Omega$) | $Z_2$ ($\Omega$) | $Z_3$ ($\Omega$) | $Z_4$ ($\Omega$) | $r_1$ ($\Omega$) | $r_2$ ($\Omega$) |
|---|---|---|---|---|---|---|
| 3.8 | 60 | 144 | 150 | 60 | 35 | 152 |
| 10.9 | 150 | 110 | 20 | 60 | 64 | 120 |

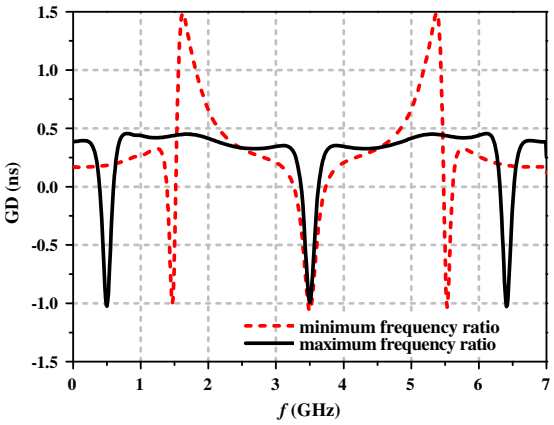


**Figure 7.** GD of the proposed NGDC with the minimum and maximum frequency ratios.

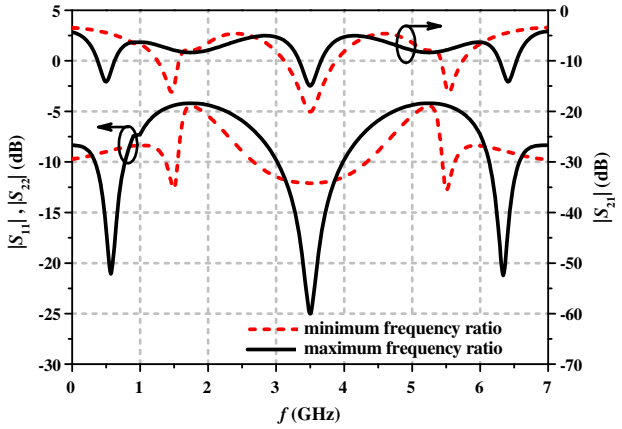


**Figure 8.** $S$-parameters of the proposed NGDC with the minimum and maximum frequency ratios.

Based on the previous analysis, the NGD operation frequency must be $f_0 = (f_1 + f_2)/2$. In order to eliminate the limitation for some practical application, a cascaded structure consisting of two units of the proposed NGDCs is shown in Fig. 9. Two NGD units have the same center frequency and different frequency ratios. The transmission lines $Z_{m1}$ and $Z_{m2}$ are used to achieve port matching. For verification, a 0.75/3.0/5.5-GHz tri-band NGDC is designed. The electrical parameters are shown in Table 2. The simulated results of $S$-parameters and GD are shown in Fig. 10. At 0.75 GHz, the GD and $|S_{21}|$ are $-1.0$ ns and $-24.9$ dB, respectively. The input/output RLs are 11.9 dB and 13.2 dB, respectively. At 3.0 GHz, the GD and $|S_{21}|$ are $-1.0$ ns and $-29.4$ dB with $|S_{11}|= -17.6$ dB and $|S_{22}|= -18.3$ dB. At 5.5 GHz, the GD and $|S_{21}|$ are $-1.0$ ns and $-24.1$ dB, respectively. The input/output RLs are 15.9 dB and 20 dB, respectively.

**Table 2.** Electrical parameters for the cascaded structure.

| $Z_{11}$ ($\Omega$) | $Z_{12}$ ($\Omega$) | $Z_{13}$ ($\Omega$) | $Z_{14}$ ($\Omega$) | $Z_{21}$ ($\Omega$) |
|---|---|---|---|---|
| 140 | 150 | 49 | 150 | 150 |
| $Z_{22}$ ($\Omega$) | $Z_{23}$ ($\Omega$) | $Z_{24}$ ($\Omega$) | $r_{11}$ ($\Omega$) | $r_{12}$ ($\Omega$) |
| 130 | 20 | 150 | 70 | 55 |
| $r_{21}$ ($\Omega$) | $r_{22}$ ($\Omega$) | $Z_{\mathrm{m1}}$ ($\Omega$) | $Z_{\mathrm{m1}}$ ($\Omega$) | $\theta_5$ |
| 83 | 277 | 80 | 70 | $\pi f/f_0$ |

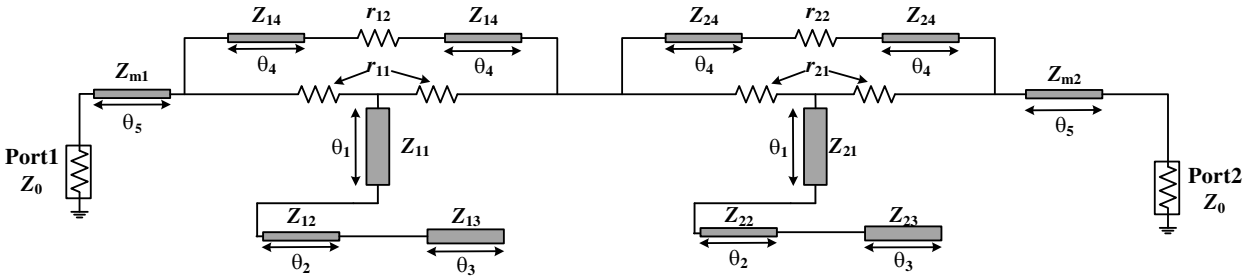


**Figure 9.** Configuration of cascading the proposed NGDCs.

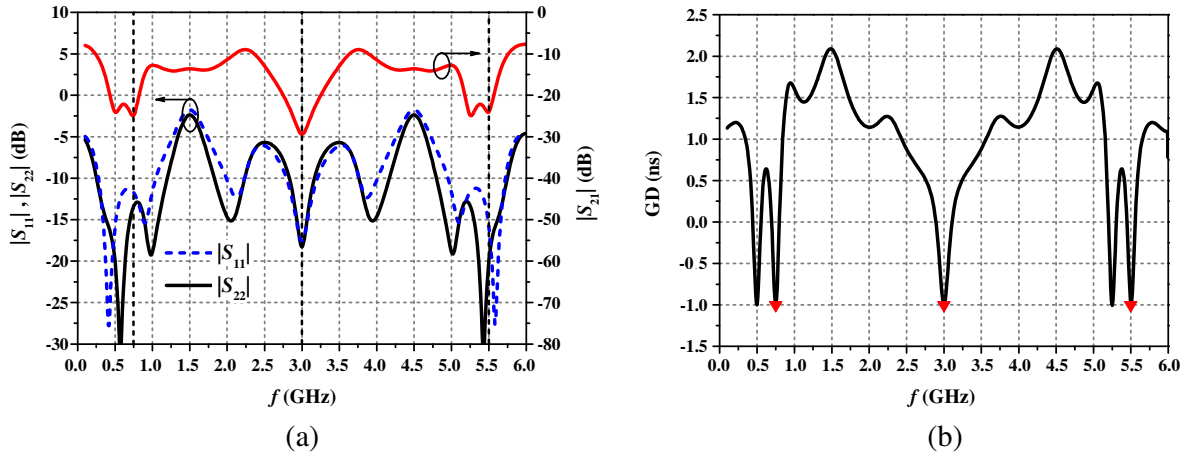


**Figure 10.** Simulated results of the cascaded structure. (a) $S$-parameters. (b) GD.

## 4. IMPLEMENTATION AND PERFORMANCE

To validate the design concept of the proposed NGDC, a tri-band NGDC is designed with $f_1 = 1.2\,\mathrm{GHz}$, $f_0 = 3.5\,\mathrm{GHz}$ and $f_2 = 5.8\,\mathrm{GHz}$. The NGDC is fabricated on a substrate with relative permittivity $\varepsilon_r = 2.55$ and thickness $h = 1.5\,\mathrm{mm}$. With the foregoing design equations and analysis, the electrical parameters are obtained as $Z_1 = 71\,\Omega$, $Z_2 = 150\,\Omega$, $Z_3 = 87\,\Omega$, $Z_4 = 150\,\Omega$, $r_1 = 61\,\Omega$, and $r_2 = 424\,\Omega$. Fig. 11(a) shows the layout of the proposed circuit. In order to eliminate the effect of the bending of microstrip lines and the coupling between them, the length and width of the microstrip lines are adjusted in the ANSYS HFSS to optimize the performance the closest to the calculated results. The physical dimensions after optimizing are $w_1 = 1.6\,\mathrm{mm}$, $l_{11} = 6.8\,\mathrm{mm}$, $l_{12} = 11.5\,\mathrm{mm}$, $w_2 = 0.3\,\mathrm{mm}$, $l_{21} = 1\,\mathrm{mm}$, $l_{22} = 3.3\,\mathrm{mm}$, $l_{23} = 11.5\,\mathrm{mm}$, $w_3 = 1.6\,\mathrm{mm}$, $l_3 = 15\,\mathrm{mm}$, $w_4 = 0.4\,\mathrm{mm}$, $l_{41} = 1\,\mathrm{mm}$, $l_{42} = 3.5\,\mathrm{mm}$, $l_{43} = 13.6\,\mathrm{mm}$, $l_{44} = 2.8\,\mathrm{mm}$, $l_{45} = 14.5\,\mathrm{mm}$, $w_p = 4.2\,\mathrm{mm}$, $l_p = 15\,\mathrm{mm}$, $r_1 = 51\,\Omega$,

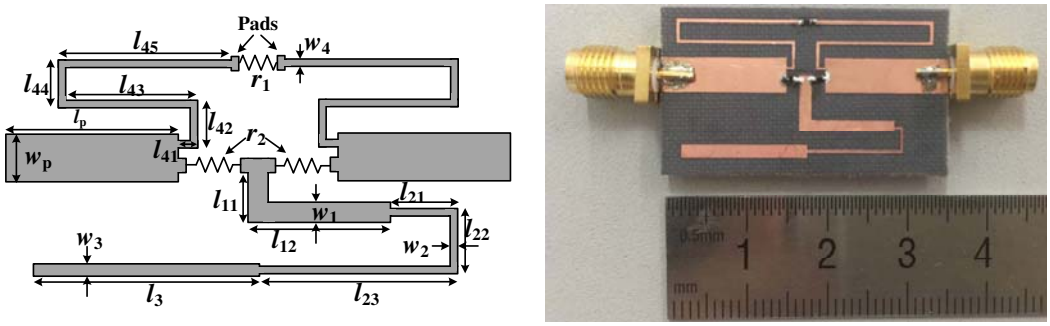


**Figure 11.** The proposed NGDC. (a) Layout. (b) Photograph.

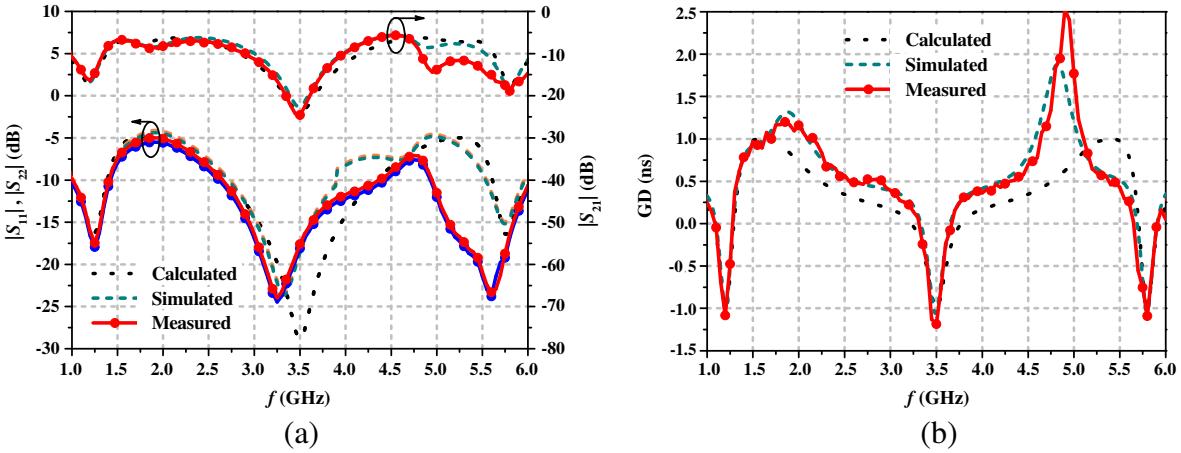


**Figure 12.** Calculated, simulated and measured results of the proposed tri-band NGDC. (a) $S$-parameters. (b) GD.

$r_2 = 499\,\Omega$. A photograph of the fabricated tri-band NGDC is illustrated in Fig. 11(b). The overall circuit dimension is 20 mm × 34.5 mm (around $0.34\lambda_g \times 0.59\lambda_g$, where $\lambda_g$ is the guided wavelength of 50-Ω TLs at the center frequency of $f_0$). The fabricated prototype is measured with an Agilent N5230A network analyzer.

Figure 12 shows the measured results of $S$-parameters and GD, along with the calculated and simulated ones for comparison. Through the optimization of microstrip-line size, the simulated and measured results of GD and $|S_{21}|$ are in agreement with the calculated results at three NGD bands. Although there are some differences in $|S_{11}|$ at $f_0 = 3.5$ GHz, good input- and output-port impedance matching characteristics are also obtained. In Fig. 12, for $f_1$ of 1.2 GHz, the measured GD and $|S_{21}|$ are −1.08 ns and −16.38 dB, respectively. The NGD fractional bandwidth (FBW) is 12.4% from 1.102 to 1.251 GHz; the flat-NGD bandwidth is 2.7% with ±8% GD fluctuation; and the input/output RL is better than 12.1 dB in the NGD bandwidth with a maximum RL of 16.09 dB. For $f_0$ of 3.5 GHz, the measured GD and $|S_{21}|$ are −1.19 ns and −24.58 dB, respectively. The NGD FBW is 8.60% from 3.351 to 3.652 GHz with a flat-NGD bandwidth of 1.4%, and the input/output RL is better than 14.7 dB in the NGD bandwidth with a maximum RL of 17.6 dB. For $f_2$ of 5.8 GHz, the measured GD and $|S_{21}|$ are −1.09 ns and −18.9 dB, respectively. The NGD FBW is 3.59% from 5.694 to 5.902 GHz with a flat-NGD bandwidth of 0.7%, and the input/output RL is better than 13.2 dB in the NGD bandwidth with a maximum RL of 16.4 dB.

Table 3 shows the comparison of the proposed tri-band NGDC with previous dual-band and tri-band designs. The proposed NGDC has better input/output port matching than the tri-band NGDC in [27], and the NGD time can be the same at the three design frequencies. Compared with the

**Table 3.** Performance comparison.

| Ref. | $f$ (GHz) | NGD (ns) | IL (dB) | RL (dB) | NGD FBW (%) | FOM | Size ($\lambda_g \times \lambda_g$) |
|---|---|---|---|---|---|---|---|
| [21] | 2.14 | −3.00 | 34.2 | 17.0 | 8.41 | 0.0105 | $0.09 \times 1.80$ |
| | 3.50 | −3.10 | 34.9 | 17.0 | 5.14 | 0.0100 | |
| [22] | 3.50 | −4.54 | 47.4 | - | 3.43 | 0.0023 | $0.36 \times 0.64$ |
| | 5.15 | −4.20 | 38.8 | - | 1.94 | 0.0048 | |
| [23] | 3.50 | −5.00 | 13.0 | - | 5.71 | 0.2237 | $0.60 \times 0.64$ |
| | 5.20 | −5.00 | 19.5 | - | 5.77 | 0.1589 | |
| [24] | 0.667 | −1.19 | 18.2 | 24.8 | 34.5 | 0.0338 | $0.13 \times 0.27$ |
| | 1.377 | −1.19 | 18.2 | 24.7 | 16.5 | 0.0332 | |
| [25] | 0.660 | −1.03 | 16.9 | 18.4 | 35.2 | 0.0338 | $0.13 \times 0.27$ |
| | 1.390 | −1.03 | 16.9 | 17.6 | 16.6 | 0.0332 | |
| [26] | 0.496 | −2.93 | 8.3 | 23.3 | 7.66 | 0.0426 | $0.19 \times 0.50$ |
| | 1.499 | −3.05 | 10.2 | 25.4 | 3.67 | 0.0519 | |
| [27] | 2.80 | −6.5 | 21 | - | 4.29 | 0.0696 | $0.387 \times 0.032$ |
| | 4.30 | −5.4 | 24 | - | 4.19 | 0.0614 | |
| | 5.80 | −3.0 | 23 | - | 4.31 | 0.0531 | |
| This work | 1.20 | −1.08 | 16.4 | 16.1 | 12.4 | 0.0252 | $0.34 \times 0.59$ |
| | 3.50 | −1.19 | 24.6 | 17.6 | 8.60 | 0.0472 | |
| | 5.80 | −1.09 | 18.9 | 16.4 | 3.59 | 0.0344 | |

previous designs [21–27], the proposed NGDC can work at three frequency bands for the practical system application (Beidou B2, WiMax, and WLAN), so it can make the tri-band system easier to realize in practice and reduce circuit size. The proposed NGDC has lower IL and greater figure of merit (FOM) than the circuits in [21, 22], where the FOM is defined as

$$\text{FOM} = |\tau(f)| \times \text{BW}_{\text{NGD}} \times |S_{21}(f)|. \tag{9}$$

Besides, the proposed NGDC has a smaller circuit size and better port-matching than the previous works in [22, 23]. Compared to the NGDC in [24, 25], the proposed NGDC has the same level of GD.

## 5. CONCLUSIONS

In this paper, a novel tri-band NGDC has been presented and self-matched without the need for external matching networks. The proposed circuit consists of three-stage series transmission lines connecting with two resistors, and a resistor connected by two transition lines. Using the proposed method, a tri-band NGDC for Beidou, WiMax, and WLAN is designed, fabricated, and measured. The proposed NGDC has better RL performance than other tri-band NGDCs. In addition, its size is also small. So it can be applied in various tri-band microwave circuits and systems.

## ACKNOWLEDGMENT

This work was supported by the National Natural Science Foundation of China (Nos. 61871417 and 51809030), the Natural Science Foundation of Liaoning Province (Nos. 2019-MS-024 and 2020-MS-127), the Liaoning Revitalization Talents Program, and the Fundamental Research Funds for the Central Universities (Nos. 3132020206 and 3132020207).

## REFERENCES


1. Ravelo, B., "Recovery of microwave-digital signal integrity with NGD circuits," *Photon. Optoelectron*, Vol. 2, No. 1, 8–16, Jan. 2013.
2. Eudes, T. and B. Ravelo, "Cancellation of delays in the high-rate interconnects with UWB NGD active cells," *Appl. Phys. Res.*, Vol. 3, No. 2, 81–88, Nov. 2011.
3. Ahn, K., R. Ishikawa, and K. Honjo, "Group delay equalized UWB InGaP/GaAs HBT MMIC amplifier using negative group delay circuits," *IEEE Trans. Microwave Theory Tech.*, Vol. 57, No. 9, 2139–2147, Sept. 2009.
4. Ahn, K., R. Ishikawa, and K. Honjo, "Low noise group delay equalization technique for UWB InGaP/GaAs HBT LNA," *IEEE Microwave Wireless Compon. Lett.*, Vol. 20, No. 7, 405–407, Jul. 2010.
5. Shao, T., Z. Wang, S. Fang, H. Liu, and Z. N. Chen, "A full-passband linear-phase band-pass filter equalized with negative group delay circuits," *IEEE Access*, Vol. 8, 43336–43343, 2020.
6. Shao, T., Z. Wang, S. Fang, H. Liu, and Z. N. Chen, "A group-delay-compensation admittance inverter for full-passband self-equalization of linear-phase band-pass filter," *Int. J. Electron. Commun.*, Vol. 123, Art. No. 153297, Aug. 2020.
7. Choi, H., Y. Jeong, C. D. Kim, and J. S. Kenney, "Efficiency enhancement of feedforward amplifiers by employing a negative Group-delay circuit," *IEEE Trans. Microwave Theory Tech.*, Vol. 58, No. 5, 1116–1125, May 2010.
8. He, L., W. Li, J. Hu, and Y. Xu, "A 24-GHz source-degenerated tunable delay shifter with negative group delay compensation," *IEEE Microwave Wireless Compon. Lett.*, Vol. 28, No. 8, 687–689, Aug. 2018.
9. Lucyszyn, S., I. D. Robertson, and A. H. Aghvami, "Negative group delay synthesiser," *Electron. Lett.*, Vol. 29, No. 9, 798–800, Apr. 1993.
10. Chaudhary, G., Y. Jeong, and J. Lim, "Miniaturized negative group delay circuit using defected microstrip structure and lumped elements," *IEEE MTT-S Int. Microwave Symp. Dig.*, 1–3, Seattle, WA, USA, Jun. 2013.
11. Chaudhary, G. and Y. Jeong, "A design of compact wideband negative group delay network using cross coupling," *Microw. Opt. Technol. Lett.*, Vol. 56, No. 11, 2612–2616, Nov. 2014.
12. Chaudhary, G. and Y. Jeong, "Negative group delay phenomenon analysis in power divider: Coupling matrix approach," *IEEE Trans. Compon. Packag. Manuf. Technol.*, Vol. 7, No. 9, 1543–1551, Sept. 2017.
13. Ravelo, B., "Negative group-delay phenomenon analysis with distributed parallel interconnect line," *IEEE Trans. Electromagn. Compat.*, Vol. 58, No. 2, 573–580, Apr. 2016.
14. Chaudhary, G., Y. Jeong, and J. Lim, "Microstrip line negative group delay filters for microwave circuits," *IEEE Trans. Microwave Theory Tech.*, Vol. 62, No. 2, 234–243, Feb. 2014.
15. Wu, C. M. and T. Itoh, "Maximally flat negative group delay circuit: A microwave transversal filter approach," *IEEE Trans. Microwave Theory Tech.*, Vol. 6, No. 6, 1330–1342, Jun. 2014.
16. Wang, Z., Y. Cao, T. Shao, S. Fang, and H. Liu, "A negative group delay microwave circuit based on signal interference techniques," *IEEE Microwave Wireless Compon. Lett.*, Vol. 28, No. 4, 290–292, Apr. 2018.
17. Chaudhary, G. and Y. Jeong, "Arbitrary terminated negative group delay circuit using signal interference concept," *Int. J. RF Microw. Comput. Aided Eng.*, Vol. 30, No. 10, 1–7, Jun. 2020.
18. Kim, K. and C. Nguyen, "A SiGe BiCMOS concurrent K/V dual-band 16-way power divider and combiner," *IEEE Trans. Circuits Syst. I: Regul. Pap.*, Vol. 65, No. 6, 1850–1861, Jun. 2018.
19. Yang, G., S. Zhang, J. Li, Y. Zhang, and G. F. Pedersen, "A multi-band magneto-electric dipole antenna with wide beam-width," *IEEE Access*, Vol. 8, 68820–68827, Apr. 2020.
20. Gómez-García, R., J. Rosario-De Jesus, and D. Psychogiou, "Multi-band bandpass and bandstop RF filtering couplers with dynamically-controlled bands," *IEEE Access*, Vol. 6, 32321–32327, Jun. 2018.

21. Choi, H., Y. Jeong, J. Lim, S. Eom, and Y. Jung, "A novel design for a dual-band negative group delay circuit," *IEEE Microwave Wireless Compon. Lett.*, Vol. 21, No. 1, 19–21, Jan. 2011.
22. Chaudhary, G., Y. Jeong, and J. Lim, "Miniaturized dual-band negative group delay circuit using dual-plane defected structures," *IEEE Microwave Wireless Compon. Lett.*, Vol. 24, No. 8, 521–523, Aug. 2014.
23. Taher, H. and R. Farrell, "Dual wide-band miniaturized negative group delay circuit using open circuit stubs," *Microwave Opt. Technol. Lett.*, Vol. 60, No. 2, 428–432, Jul. 2018.
24. Shao, T., S. Fang, Z. Wang, and H. Liu, "A compact dual-band negative group delay microwave circuit," *Radioengineering*, Vol. 27, No. 4, 1070–1076, Dec. 2018.
25. Shao, T., S. Fang, Z. Wang, H. Liu, and S. Fu, "A novel dual-band negative group delay microwave circuit," *IEEE Radio Wirel. Symp. (RWS)*, 1–3, May 2019.
26. Meng, Y., Z. Wang, S. Fang, T. Shao, H. Liu, and Z. Chen, "Dual-band negative group delay microwave circuit with low signal attenuation and arbitrary frequency ratio," *IEEE Access*, Vol. 8, 49908–49919, Mar. 2020.
27. Xiao, J. and Q. Wang, "Individually controllable tri-band negative group delay circuit using defected microstrip structure," *Cross Strait Quad-Regional Radio Sci. Wirel. Technol. Conf.*, 1–3, Taiyuan, China, 2019.
28. Ravelo, B., "Resistive and distributed multiband NGD active circuit," *URSI Asia-Pac. Radio Sci. Conf. (URSI AP-RASC)*, 1–4, South Korea, Aug. 2016.
29. Ravelo, B., "Innovative theory on multiband NGD topology based on feedback-loop power combiner," *IEEE Trans. Circuits Syst. II: Express Briefs*, Vol. 63, No. 8, 738–742, Aug. 2016.